Geophysical Research Letters

RESEARCH LETTER
10.1029/2024GL113214

The 2024 Fentale Diking Episode in a Slow Extending Continental Rift

D. Keir[1,2], A. La Rosa[3], C. Pagli[3], H. Wang[4], A. Ayele[5], E. Lewi[5], F. Monterroso[6], and M. Raggiunti[7]

[1]School of Ocean and Earth Science, University of Southampton, Southampton, UK, [2]Department of Earth Sciences, University of Florence, Florence, Italy, [3]Department of Earth Sciences, University of Pisa, Pisa, Italy, [4]College of Natural Resources and Environment, South China Agricultural University, Guangzhou, China, [5]Institute of Geophysics, Space Science and Astronomy (IGSSA), Addis Ababa University, Addis Ababa, Ethiopia, [6]Institute for Electromagnetic Sensing of Environment (IREA), National Research Council (CNR), Naples, Italy, [7]National Institute for Geophysics and Volcanology (INGV), Rome, Italy

Abstract Dikes can contribute to rifting, but the space-time behavior and role of magma in young and slowly extending continental rifts is unclear. We use InSAR and seismicity during the 2024 Fentale intrusion in the Main Ethiopian rift (MER) to understand magma-assisted rifting at slow extension rates (5 mm/yr). From 2021 to mid-2024, the Fentale Volcanic Complex (FVC) uplifted up to 6 cm. From mid-September 2024, upper crustal diking started northwards along the rift, initially with subdued seismicity. From late-September to early November, dike opening increased to ∼2 m and propagated a total of ∼14 km north, causing increased seismicity from normal faulting. The dike made ∼90% of the total geodetic moment, with the rest from faulting. The character of the event is similar to rifting episodes at mid-ocean ridges and demonstrates that episodic diking can occur in young, slow extending continent rifts but must be more infrequent.

Plain Language Summary The continents on Earth move away from each other forming a rift valley. It is commonly accepted that the rift valley forms from fracturing of the Earth, forming geological faults which make a low lying downfaulted rift valley. The fracturing and faulting cause the rift to get wider through time. However, many rift valleys such as in East Africa have many active volcanoes, below which molten rock called magma moves from depth. The role and behavior of the magma in potentially helping the rift to grow and evolve is not well understood. In this study we map the motions of the Earth's surface during intense earthquake activity in September–November 2024 at a volcano (Fentale) in Ethiopia, using satellite images and seismograph recordings. The information shows that a roughly 14 km long blade of magma was injected from the volcano into the rift, widening it 2 m in a few weeks. The results suggest that rapid motion of magma every few hundred years helps continents to divide.

Key Points:

- A seismic sequence with several >M5 earthquakes occurred in the Fentale region of the Ethiopian rift during September–November 2024
- InSAR models show ground motion dominated by rapid dike intrusion along the rift, causing normal faulting
- The ∼2-m-width of the dike and historical records of volcanic activity suggests episodic diking episodes every few hundred years

Supporting Information:

Supporting Information may be found in the online version of this article.

Correspondence to:

D. Keir,
d.keir@soton.ac.uk

Citation:

Keir, D., La Rosa, A., Pagli, C., Wang, H., Ayele, A., Lewi, E., et al. (2025). The 2024 Fentale diking episode in a slow extending continental rift. *Geophysical Research Letters*, *52*, e2024GL113214. https://doi.org/10.1029/2024GL113214

Received 23 OCT 2024
Accepted 21 JAN 2025

Author Contributions:

Conceptualization: D. Keir, A. La Rosa, C. Pagli, A. Ayele, E. Lewi
Formal analysis: D. Keir, A. La Rosa, C. Pagli, A. Ayele, F. Monterroso, M. Raggiunti
Methodology: C. Pagli, H. Wang, F. Monterroso
Software: H. Wang
Supervision: C. Pagli
Visualization: E. Lewi
Writing – original draft: D. Keir, A. La Rosa, C. Pagli, H. Wang, A. Ayele, E. Lewi, F. Monterroso
Writing – review & editing: D. Keir, A. La Rosa, C. Pagli, H. Wang

1. Introduction

The majority of continental rifts, such as the East African rift (EAR), open at slow extension rates, <1 cm/yr (Brune et al., 2016). At these slow rates, classic models of mantle decompression melting suggest limited, or no, magma supply, even above a moderately hot mantle plume (e.g., Bown & White, 1995). Such models have led to debate whether the mechanism of magma-assisted rifting (Bialas et al., 2010) is relevant for young continental rifts (Calais et al., 2008). In addition, the relative lack of direct observations of active magma intrusion in slow rifts, has led to uncertainty regarding the behavior of diking in space and time (Asfaw et al., 1992). Here, we present new observations and models of active dike intrusion during September–November 2024 from InSAR and seismicity near Fentale caldera in the slowly extending Main Ethiopian rift (MER) of East Africa to address these questions (Figure 1).

The MER strikes NNE to NE across the Ethiopian dome into Afar causing extension between the Nubian and Somalian plates at around 5 mm/yr in an ∼E-W direction (Birhanu et al., 2016) (Figure 1). The MER is thought to have initiated at 10–20 Ma, with rifting limited to the NE striking border faults for most of the rift history (Wolfenden et al., 2004). In-rift localization of faulting and increase in volcanism occurred since ∼2 Ma (Ebinger & Casey, 2001). The current plate boundary zone is thought to be marked by the in-rift, NNE striking, right stepping en-echelon volcanic segments which are similar in width (∼20–30 km), length scale (50–70-km), and surface morphology to those in Afar and Iceland (Ebinger & Casey, 2001; Siegburg et al., 2023). The 2024

10.1029/2024GL113214

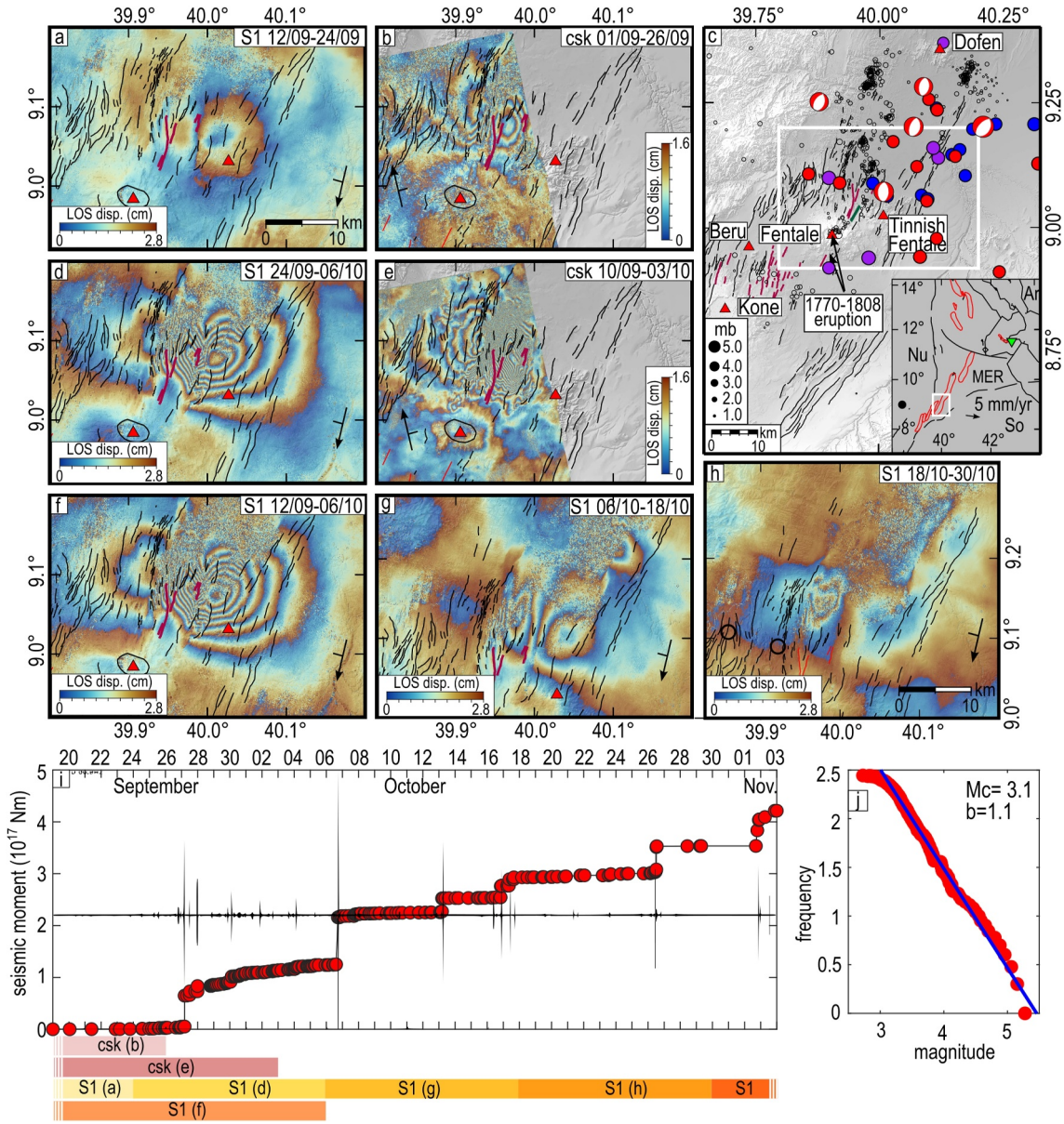

Figure 1. (a–h) Key interferograms of the study and location of the FVC in the MER. (c) Location map with the white box shows the extent of all interferograms with the exception of (g) and (h). Red triangles are Holocene volcanoes of which Fentale caldera is one. Faults are marked with black lines and eruptive fissures with red lines. The thick pink line is the 2015 dike from Temtime et al. (2020). Black dots are microseismicity during 2001–2003 from Keir et al. (2006). Red, blue and purple dots are respectively the NEIC, EMSC, and GFZ catalogs of the seismic swarm during September–November 2024. Moment tensors are from the GFZ catalog. (a, b, d–h) Key wrapped interferograms are shown as (a) S1 during the start of the sequence from 12 to 24 September, (b) CSK for 1–26 September, (d) S1 for 24 September to 6 October 03:09 (UTC), (e) CSK for 10 September to 3 October, (f) CSK for 12 September to 6 October 03:09 (UTC) and (g) S1 for 6 October 03:09 (UTC) to 18 October, (h) S1 for 18–30 October. Negative LOS is motion of the ground toward the satellite. (i) Is cumulative seismic moment release through time measured from the >250 earthquakes recorded at the seismic station ATD. Red dots are individual earthquakes. The black line is the continuous vertical seismogram from ATD filtered 0.02–1 Hz in order to show only the earthquakes from Fentale. (j) Gutenberg-Richter plot showing magnitude-frequency distribution of the earthquake swarm, with Mc of 3.1 and *b*-value of 1.1.

activity occurred in the Fentale-Dofen volcanic segment, at the southern end of which are Fentale caldera (most recent caldera eruption at 168 ± 38 ka) and Tinish Fentale volcanic center, that combined make the Fentale Volcanic Complex (FVC) (Fontijn et al., 2018) (Figure 1). The FVC has mostly rhyolitic pyroclastic deposits and post-caldera obsidian and rhyolite flows (Fontijn et al., 2018), with more spatially limited fissural basalts (Siegburg et al., 2023; Williams et al., 2004). Historical eruptions are the 1770–1808 fissural basalts from Tinish Sabober cone on the southern flank of Fentale caldera (Harris, 1844; Siegburg et al., 2023) (Figure 1), and flows

of similar age in the neighboring Kone (1808–1810) and Boset (1812–1919) volcanic segments, indicating a regional rifting episode ∼200 years ago (Siegburg et al., 2023). The crust near Fentale is 30-km thick (Maguire et al., 2006), with microseismicity studies showing the brittle layer is ∼15-km thick (Keir et al., 2006; Raggiunti et al., 2023).

Constraints on the role and dynamics of dike intrusion during extension come mainly from more rapidly extending (>1 cm per year) rifts near breakup, and from the mid-ocean ridge system. Rifting episodes such as the 2005–2010 Dabbahu episode in Afar (Barnie et al., 2016; Wright et al., 2006), and 2021-ongoing Fagradalsfjall episode in Iceland (Sigmundsson et al., 2024) show ∼meter-wide and ∼10–30–km-long dikes that laterally propagate over hours to weeks, consistent with basaltic magma as observed during the dike fissuring (Barnie et al., 2016; Sigmundsson et al., 2024). In contrast and despite the length of the EAR, only two dike intrusions have been observed, both of which were unusual. In 2007, diking in the Natron rift was triggered by slow slip on a rift-bounding normal fault (Calais et al., 2008). In 2015, slow (10 months) NE directed growth of a 6-km-long dike just north of Fentale crater was modeled as a rhyolitic intrusion (Ayele et al., 2024; Temtime et al., 2020) (Figure 1).

2. Seismicity

Global seismic catalogs such as the National Earthquake Information Center (NEIC), European-Mediterranean Seismic Centre (EMSC), and Geofon GFZ catalogs reported 3 earthquakes near the FVC on 27 September 2024, with the largest being M4.9–5.2 at 04:36 (UTC) (Figures 1a and 1b; Table S1 in Supporting Information S1). These were followed by a further 9 earthquakes during 30 September to 2 November, the largest of which was an M4.9–5.3 on 6 October at 17:10 (UTC) (Figure 1; Table S1 in Supporting Information S1). The Geofon GFZ seismic catalog reports moment tensors for both these two earthquakes with normal faulting on N to NE striking nodal planes, but with some of the magnitude estimates being over M5 (mb 5.2 for 27 September, and M_W 5.3 for 6 October) (Figure 1; Table S1 in Supporting Information S1). The 3 earthquakes in early November of M_W 4.6–4.8 also have similar normal faulting mechanisms (Figure 1; Table S1 in Supporting Information S1).

The earthquakes reported on the global catalogs have formal horizontal error bars of up to ±14 km and therefore have inaccurate locations (Figures 1a and 1b; Table S1 in Supporting Information S1), and they only scratch the surface of the timescales of the seismic sequence. To improve the temporal record of seismicity we analyzed the continuous seismic data from seismic station at ATD in Djibouti, which was streaming data real time during the sequence (Figure 1). ATD is part of the GEOSCOPE network (Institut de physique du globe de Paris (IPGP) and Ecole et Observatoire des Sciences de la Terre de Strasbourg (EOST), 1982). We inspected data from the start of September 2024 through to early November and found 278 additional earthquakes with the ∼50-s time difference between the P and S waves similar to the earthquakes reported by the global catalogs. We computed M_L from amplitude measurements on simulated Wood-Anderson seismograms averaged from both horizontal components. We used a distance of 415 km from ATD to a point at the middle of the InSAR derived deformation signal, and the distance correction for Ethiopia as in La Rosa et al. (2023). Varying the epicentral distance by ±10 km in line with the length of the deformation zone only changes the computed magnitude by a maximum of ±0.02 magnitude units. Our computed M_L are very similar across all earthquakes to magnitudes quoted by the Geofon GFZ catalog (Table S1 in Supporting Information S1). Our local magnitudes for the 2 largest earthquakes are M_L 5.2 for 27 September and M_L 5.3 for 6 October (Table S1 in Supporting Information S1).

We compute the seismic moment release by assuming a 1:1 relationship between M_L and M_w and then compute M_o using Hanks and Kanamori (1979). We also used the Gutenburg-Richter relationship to compute a completeness magnitude of M_L 3.1 and a b-value for the swarm of 1.1 (Figure 1j). The seismic moment release through time shows the first earthquake that ATD detected was on 19 September, with subdued seismicity through to 24 September (Figure 1i). Earthquake numbers increased from 25 September but initially with smaller ($M < 4$) earthquakes, but then from 27 September included the larger globally recorded earthquakes (Figure 1i). Seismic moment release totals 1.3×10^{17} Nm for the time period to 6 October 03:09 (UTC), which by 18 October increased to 2.8×10^{17} Nm mainly during the second >M5 earthquake on 6 October 17:10 (UTC) (Figure 1i). By the end of the activity on 2 November seismic moment release totaled 4.2×10^{17} Nm (Figure 1i).

3. InSAR Data Analysis and Results

For InSAR analysis of the sequence we created interferograms using radar acquisitions from Sentinel-1 (S1) satellite (European Space Agency) in descending (track 079) and ascending geometries (track 089), and COSMO-SkyMed (CSK) satellite (Italian Space Agency) in ascending geometry (Figures 1a–1h) (Tables S3 and S4 in Supporting Information S1). We also analyzed S1 data to constrain ground deformation 3 years prior to the event. All the interferograms were processed with the InSAR Scientific Computing Environment (ISCE2) software package (Rosen et al., 2012). For the processing, we co-registered the SLCs and removed the topographic phase using a 1 arc-sec (∼30 m resolution) SRTM DEM (Farr et al., 2007). We then filtered the interferograms using a Goldstein adaptive power spectral filter with strength of 0.5 (Goldstein & Werner, 1998). Finally, we unwrapped the interferograms using the ICU branch cut algorithm (Goldstein et al., 1988; https://github.com/isce-framework/isce2-docs) and geocoded them using the 1 arc-sec SRTM DEM.

The first signs of significant ground motions occurred ∼10 km NE of Fentale caldera and are visible in an S1 interferogram spanning 12–24 September 2024 with a three-lobed pattern of up to one fringe with a central area of range increase (motion away from the satellite), a main eastern side lobe of range decrease (motion toward the satellite) and a subtle western lobe of range increase (Figure 1a). However, up to six fringes arranged in the same pattern are visible between 24 September and 6 October 03:09 (UTC) with sharp range increase in the central area and discontinuous fringes at its margins (Figures 1d and 1e). Finally, waning of the deformation occurs between 6 and 18 October and 18–30 October when the pattern extends further north but decreases to a couple of fringes (Figures 1g and 1h). The final interferogram showing deformation is 30 October to 11 November (Figure S2 in Supporting Information S1). CSK interferograms allow us to capture the spatio-temporal evolution of the dike in descending geometry but partially cover the deformation signal (Figures 1b and 1e).

To explain the observed deformation patterns, we assumed shear and tensile dislocations (Okada, 1985) in a conventional elastic half space with a Poisson's ratio of 0.25 and a shear modulus of 30 GPa. The source geometry is inferred using a non-linear Monte-Carlo-type simulated annealing inversion (Cervelli et al., 2002) assuming uniform dike opening and fault slip (Figure S1; Table S2 in Supporting Information S1). We then applied least squares inversion to determine the spatially variable dike opening and fault slip distribution, after subdividing the dislocation planes into 0.5 km × 0.5 km patches (Figures 2 and 3).

For the period of the sequence from mid-September to 6 October 03:09 (UTC) for which we have both the S1 descending and the CSK ascending interferograms, we jointly invert them to derive the sources of deformation. We inverted CSK interferogram spanning 10 September–3 October (Figure 1e) and a S1 interferogram spanning a similar period, 12 September–6 October. For S1 we added together interferograms in Figures 1a and 1d to obtain better coherence compared to the direct interferogram (Figure 1f). Our best-fit model with spatially variable dike opening and fault slip consists of a dike and two normal faults above it (Figures 2d–2i and 3b). The dike strikes N15°E, is ∼11-km-long, ∼6-km-high, reaching ∼3-km below the surface with up to ∼1.8 m of opening, giving a total volume of intruded magma of ∼0.08 km^3 (Figures 2d–2i). We estimated 0.39 and 0.14 m of slip on the two graben forming normal faults, with M_w 5.4 for the fault in the east, and M_w 4.9 for the fault in the west (Figures 2d–2i). The total fault related moment is 1.8×10^{17} Nm, while the total moment from both faults and dike is 2×10^{18} Nm. Models including a single dike or a dike and one fault were also tested but gave a worse fit.

To model the initial part of the sequence we also inverted for variable dike opening the S1 interferogram spanning 12–24 September (Figure 1a). For this modeling we kept the dike plane fixed to the results found with the joint inversion of CSK and S1. We found that magma was first injected to ∼3-km-long at the southern end of the intruded area, causing a maximum opening of only ∼0.7 m, while reaching ∼3 km depth (Figures 2a–2c and 3a). This suggests magma ascended to its final depth during the initial part of the intrusion, while dike opening and northward migration occurred after 24 September.

To model the latter part of the sequence, we used the same approach of keeping the dike plane fixed but included faults at appropriate places. Between 6 and 18 October (Figure 1g), the results show that the northern half of the dike fattened by half a meter (Figures 2j–2l and 3c). An east dipping normal fault on the western flank of the dike with 0.3 m of slip is required to explain the magnitude of subsidence above the dike (Figures 2i–2l and 3c), which cannot be explained by a dike only model. In this phase, the fault related moment is 8.9×10^{16} Nm (M_w 5.3), and the total fault and dike moment is 8.3×10^{17} Nm. During 18–30 October the dike propagated ∼3-km northward, with two west dipping normal faults NE of it along the rift (Figures 2m–2o and 3d), with both dike width and fault

10.1029/2024GL113214

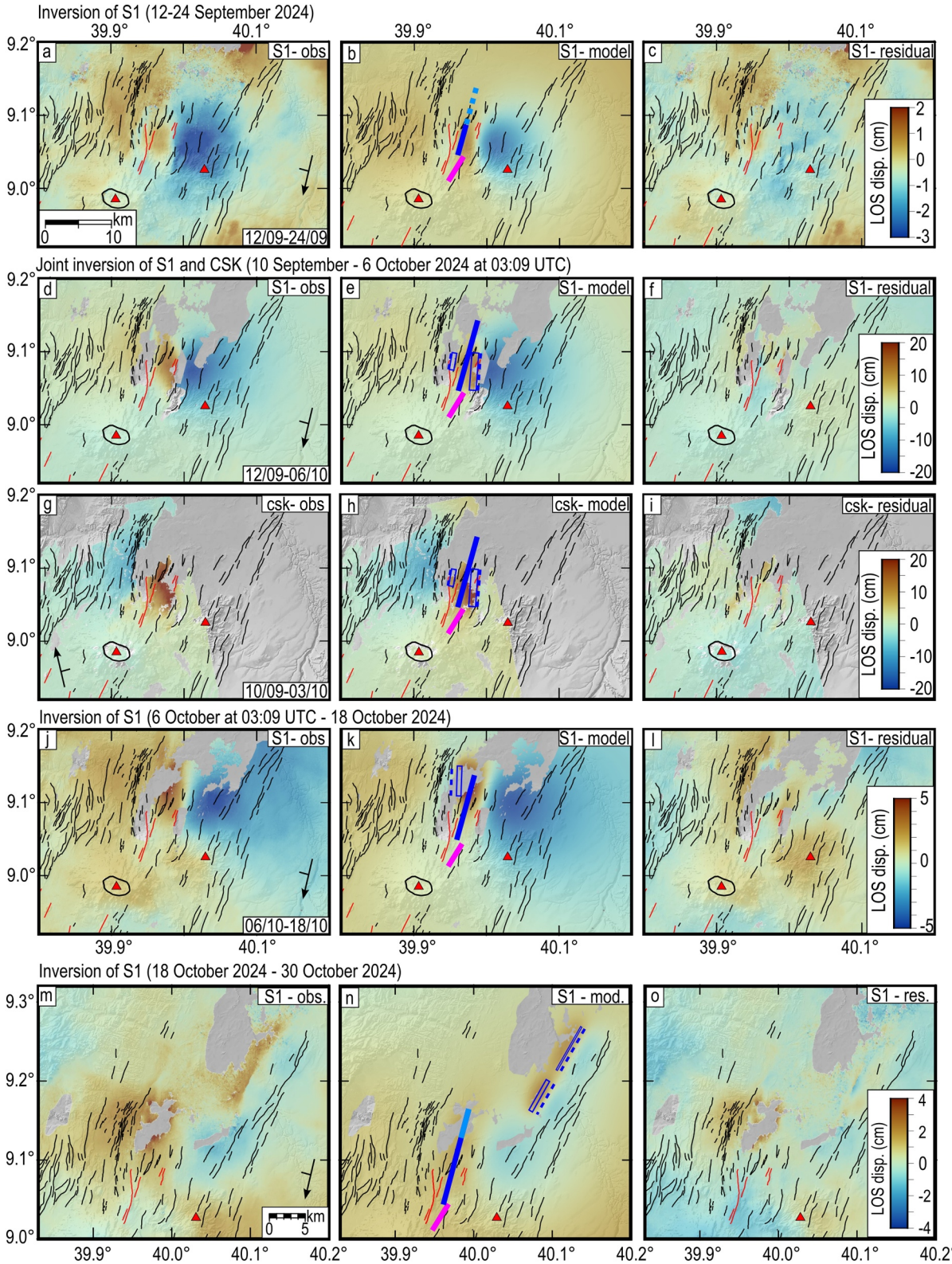

Figure 2.

slip increasing further into early November (Figure S2 in Supporting Information S1). The dike moment for 18 October to 11 November is 5.1×10^{17} Nm, while fault related moment is 1.8×10^{17} Nm (M_w 5.5). Seismicity stopped in early November (Figure 1i), and interferograms after 11 November show no deformation. The total dike volume of the full sequence is ~0.11 km^3.

To find deformation precursors to the dike we analyzed the S1 series of interferograms from 7 January 2021 to 12 September 2024. We calculated a total of 200 interferograms spanning 12–48 days and these were analyzed using the Π-RATE open-source code to estimate the average rate map, time series and their associated uncertainties (Figures S5 and S6 in Supporting Information S1) (Wang et al., 2012). For this analysis we estimate orbital errors using a linear model and the APS (Atmospheric Phase Screen) by Gaussian temporal smoothing of 2 months, followed by a spatially low-pass Butterworth filter with a window size as the wavelength of the noise variance. We then inverted for the least square average rate map and time-series using a Laplacian smoothing factor. Our rate map (Figure S6 in Supporting Information S1) and cumulative time-series maps (Figures S5a–S5l in Supporting Information S1) show that a signal of range decrease up to 5.5 cm consistent with uplift, occurred across a broad region of the FVC including the eastern flank of Fentale caldera and to ~8 km north along the rift. The uplift rate was fairly regular from 2021 to May 2024, when it stopped and then reversed into range increase, consistent with subsidence along the rift (Figure S5 in Supporting Information S1).

4. Discussion

We used InSAR and seismicity to identify and measure the deformation during a seismic swarm in September–November 2024 near the FVC, and for 3 years before it. We analyzed the time history of deformation and used elastic modeling to quantify magma motions and normal faulting. The overarching result is that the deformation is primarily magmatic in origin. From January 2021, the FVC showed ~16 mm/yr of uplift followed from April 2024 by minimal (<1 cm) subsidence (Figures S5 and S6 in Supporting Information S1). The deformation was gradual and not accompanied by measurable seismicity. The intensity and type of deformation changed from mid-September to 24 September 2024 with models of InSAR showing initial intrusion of a ~3-km-long dike starting from 10 km NE of Fentale (Figures 2a–2c and 3a), with the intrusion accompanied by low intensity and magnitude ($M < 3.5$) seismicity (Figure 1i). From 24 September to 30 October, deformation progressively extended further north and became more complex (Figures 2d–2l and 3b–3d). Our models suggest that the dike increased opening to ~2 m, and extended ~11 km further north, and was accompanied by faulting above the dike and beyond its northern tip (Figures 2d–2o and 3b–3d). The modeling combined with the magnitude and intensity of the seismicity suggest dike propagation and opening was most rapid during late September into the first week of October (Figure 1i; Figure S4 in Supporting Information S1).

The InSAR models show that rift opening was primarily caused by the dike, accounting for over ~90% of the total moment release. However, the models do also require normal faults to explain the deformation field. In our model to 6 October 03:09 (UTC), the first >M5 earthquake on 27 September is modeled by slip equivalent to M_w 5.4, compared to M_L 5.2 measured seismically (Figure 3b; Tables S1 and S2 in Supporting Information S1). The smaller fault in the model is M_w 4.9, likely associated with some, or all, the subsequent three M4.5–4.6 earthquakes during 27–30 September (Figure 3b; Table S1 in Supporting Information S1). This model has 1.8×10^{17} Nm of fault slip (equivalent to a single M5.5 earthquake), a bit more than the 1.3×10^{17} Nm (equivalent to M_w 5.4) measured seismically over the same time period. From 6 October 03:09 (UTC) to 18 October, we model normal fault slip equivalent to M_w 5.3, the same as the seismically recorded magnitude of the earthquake on 6 October 17:10 (UTC) (Figure 3c; Tables S1 and S2 in Supporting Information S1). For 18 October–early November, the fault slip in the models and observed seismically is also 1.8×10^{17} Nm and 1.3×10^{17} Nm, respectively. Discrepancies of 0.1–0.2 magnitude units for co-seismic slip modeled from geodesy above that

Figure 2. Observed unwrapped interferograms, model, and residuals for the spatially variable opening models that are shown in 3D in Figure 3. The panel rows are (a–c) S1 for 12–24 September 2024, with the 3D model shown in Figure 3a. (d–i) Joint inversion of S1 and CSK for the time period 10 September to 6 October 03:09 (UTC) 2024 with the 3D model shown in Figure 3b. The panels (d–f) show the S1 results, and panels (g–i) the results for CSK. (j–l) S1 for 6 October 03:09 (UTC) to 18 October 2024, with the 3D model shown in Figure 3c. (m–o) S1 for 18–30 October 2024, with the 3D model shown in Figure 3d. Note the variable colorbar of each row. Black and red lines are faults and fissures, respectively. The red triangles are the Fentale and Tinnish Fentale volcanoes. Black arrows in the observations are the satellite orbits and the ticks gives the viewing geometry. The thick blue lines in the models are the modeled dike. In (b) the dashed part of the dike has no opening yet, while in (n) the new dike during 18–30 October is shown in lighter blue, while the blue squares and the dashed lines are the faults and their projection at the surface, respectively. The thick magenta line is the 2015 dike from Temtime et al. (2020).

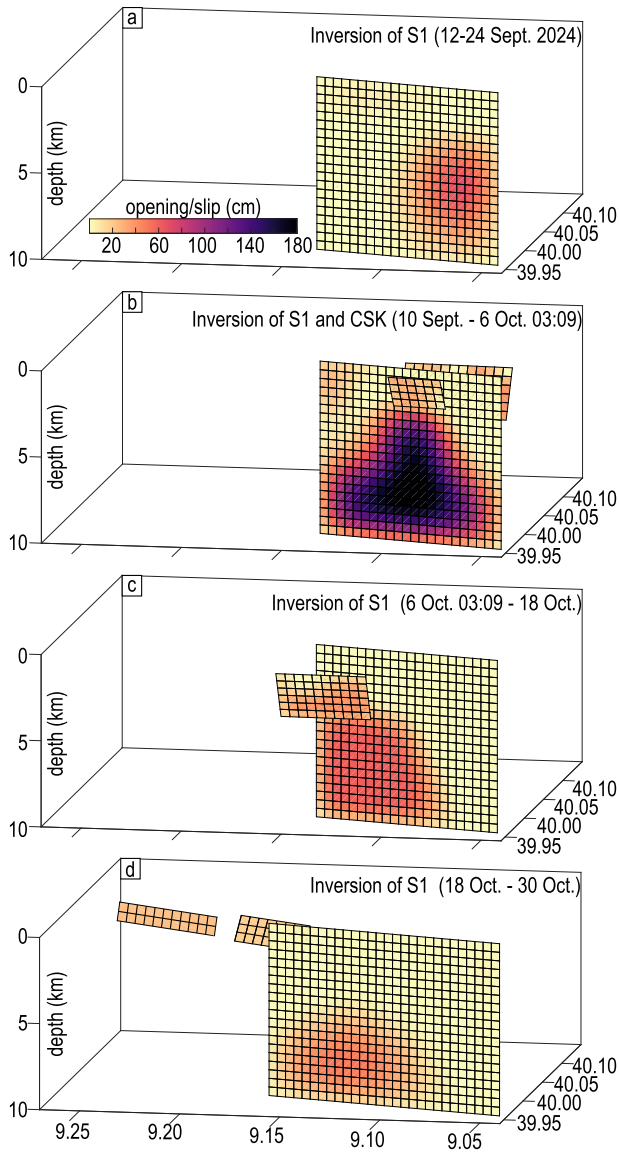

Figure 3. 3D views of the variable opening and slip models shown in Figure 2. (a) Is from inversion of S1 data from 12 to 24 September 2024 during which there is just a dike. (b) Is from joint inversion of S1 and CSK spanning 10 September 2024–6 October 03:09 (UTC) 2024 in which both a dike and two normal faults are required. The dike has migrated northward and fattened. (c) Is from the inversion of S1 from 6 October 03:09 (UTC) to 18 October 2024 which shows the northern end of the dike has fattened, and there was slip on a new fault. (d) Is from inversion of S1 of 18–30 October showing the dike migrated north and induced new fault slip NE of it.

measured seismically are common globally, and mainly interpreted as due to a slow component of fault slip not captured seismically (Weston et al., 2012). The timing and shallow depth of faulting above and ahead of the dike strongly suggests the earthquakes were triggered by diking, similar to other rifting episodes in Iceland and Afar (e.g., Keir et al., 2009; Sigmundsson et al., 2024).

The dike reached its 14 km length during the initial 6 weeks of the event, which is a minimum propagation rate of ∼0.004 m/s, and a magma flux of ∼0.003 km^3/day. However, some incremental periods of deformation suggest propagation rates and magma flux were higher, to a minimum of ∼0.02 m/s and 0.01 km^3/day respectively (Figure S4 in Supporting Information S1). These rates are at the slow end of the range (∼0.1–1 m/s) typically observed during the subaerial rifting episodes in Iceland and Afar (Grandin et al., 2011; Keir et al., 2009; Sigmundsson et al., 2024). Where they erupted, these almost all show mafic magmas (Barnie et al., 2016; Sigmundsson et al., 2024), and we therefore interpret the 2024 Fentale dike to be likely basaltic. In contrast, this is much faster than the 2015 Fentale intrusion, which migrated ∼6 km over 10 months with a flow rate consistent with a rhyolitic dike (Temtime et al., 2020). The contrasting magma types between the 2015 and 2024 intrusions suggest the plumbing system has been recharged by new mafic magma since 2015, an interpretation consistent with the 3-years of gradual uplift at the FVC prior to the 2024 intrusion (Figures S3 and S4 in Supporting Information S1).

The magma dominated deformation directly demonstrates that diking can accommodate significant extension in young and slow extending continental rifts. Magma intrusion can initiate at lower differential stresses than shear slip on a fault (Bialas et al., 2010; Ebinger & Casey, 2001), and therefore if magma is available then diking is the favored mode of rifting (Ebinger & Casey, 2001). For the 5 mm/yr long-term extension rate in the MER, a 2-m-wide dike accommodates ∼400 years of plate boundary strain accumulation. The observed dike width is typical of the ∼meter-scale global average dike widths (e.g., Qin & Buck, 2008), and similar to the widths modeled for the 2007 Natron (Calais et al., 2008) and 2015 Fentale intrusions (Temtime et al., 2020). Assuming all the extensional stress is relieved by diking then we expect several-hundred-year time intervals between rifting episodes if the extension rates are slow. This is broadly consistent with the historical record of the last major rifting episode ∼200–250 years ago (Siegburg et al., 2023; Williams et al., 2004). Basaltic fissuring ∼1770–1808 from Tinish Sobober, SE of Fentale (Harris, 1844) (Figure 1) and fresh flows in the neighboring Kone (1808–1810—historical record) and Boset (1812–1919—carbon dating) volcanic segments have been interpreted as a rifting event. The relatively low seismicity and smaller than expected strain rates within the MER plate boundary zone was recognized by Asfaw et al. (1992), who argued that episodic dike intrusion might be an important mode of extension. Our results now directly demonstrate that episodic dike intrusion is important in continental rifts, with the slow rates of extension making these episodes very infrequent.

5. Conclusions

We present InSAR data and models combined with seismicity during the September–November 2024 Fentale dike intrusion in the Main Ethiopian rift (MER), to understand magma-assisted rifting at slow (5 mm/yr) rates of plate motion. Starting at the beginning of 2021, the FVC experienced protracted unrest, with 6 cm uplift across a broad region. The uplift at the volcanic center stopped in April 2024. Dike intrusion to the north of Fentale started

in mid-September, and propagated upward and northward over several weeks, eventually forming a NNE striking, 14-km-long and ~2-m-wide dike. The dike induced normal faulting mostly after 26 September, when the dike propagated most rapidly along the rift. Dike intrusion accommodated ~90% of the total moment, with the remainder from normal fault slip. The dike shows similar scaling to examples from rifts and ridges with more rapid extension rates, with simple calculations showing that the slower rate of plate extension results in lower frequency of diking episodes. The few hundred-year repeat timescales of rifting episodes that we calculate is broadly consistent with the two centuries since the last major rifting episode in this section of the rift.

Inclusion in Global Research Statement

The manuscript has been written with the Institute of Geophysics, Space Science, and Astronomy (IGSSA) of Addis Ababa University (AAU) (authors Ayele and Lewi). The IGSSA is the official geophysical monitoring agency of Ethiopia, and have used the results to inform Ethiopian media and both regional and federal government officials. Authors from IGSSA have contributed to study designing, interpretation and writing.

Conflict of Interest

The authors declare no conflicts of interest relevant to this study.

Data Availability Statement

The NEIC catalog (USGS, 2024) is available at https://earthquake.usgs.gov/earthquakes/search/. GEOFON catalog (Quinteros et al., 2021) is available at https://geofon.gfz-potsdam.de/eqinfo/. ATD seismic data is from Earthscope https://service.iris.edu/irisws/timeseries/docs/1/builder/. ATD is in the GEOSCOPE(G) network (https://doi.org/10.18715/GEOSCOPE.G) (IPGP and EOST, 1982). Sentinel-1 Single Look Complex (SLC) acquisitions are from the European Space Agency (ESA) and Copernicus programme (Copernicus Sentinel data, 2024). Files accessed through Alaska Satellite Facility (ASF) Data Search Vertex https://search.asf.alaska.edu/#/. COSMO-SkyMed (CSK) interferograms processed at Univ.Pisa (La Rosa et al., 2024) under license of the Italian Space Agency (ASI)—Original COSMO-SkyMed Product—©ASI—(2024). CSK data archived on the Open Science Framework (OSF) repository (https://osf.io/), at https://osf.io/vdk8q/?view_only=7f572c7-c5a434b9c83a1d905286b9f75. InSAR Scientific Computing Environment (ISCE) v2 (Rosen et al., 2012) is open source and provided by NASA-JPL at https://github.com/isce-framework/isce2. The Π-RATE software (Poly-Interferogram Rate And Time-series Estimator) (Wang et al., 2012) is open source and available at https://www.phimaging.com/software/pirate/. The SRTM 30 m DEM (NASA SRTM, 2013) is from NASA Earthdata repository at https://search.earthdata.nasa.gov/search?q=SRTM. Figures are produced using Matlab 2022 (The MathWorks Inc., 2022) and the Generic Mapping Tools (GMT) software v6.0.0 (Wessel et al., 2019).

Acknowledgments
DK acknowledges NERC Grant NE/L013932. COSMO-SkyMed interferograms processed at Univ.Pisa, Italy under a license of the Italian Space Agency (ASI); Original COSMO-SkyMed Product—©ASI—(2024). ISP (International Science Program) supports the Ethiopian seismic network. CP and ALR acknowledge the SpaceItUp project funded by ASI and MiUR, contract n.2024-5-E.0—CUP n.I53D24000060005. HW supported by NSF of China (42274001) and the Associates Program from ICTP/Simons Foundation (284558FY19). FM acknowledges GeoSciences IR—PNRR M4C2 Investimento 3.1- IR0000037.

References

Asfaw, L. M., Bilham, R., Jackson, M., & Mohr, P. (1992). Recent inactivity in African rift. *Nature*, *357*(6378), 447. https://doi.org/10.1038/357447a0

Ayele, A., Luckett, R., Baptie, B., & Whaler, K. (2024). The 2015 earthquake swarm in the Fentale volcanic complex (FVC): A geohazard risk for Ethiopia's commercial route to the Djibouti port. *Journal of African Earth Sciences*, *213*, 105236. https://doi.org/10.1016/j.jafrearsci.2024.105236

Barnie, T. D., Keir, D., Hamling, I., Hofmann, B., Belachew, M., Carn, S., et al. (2016). A multidisciplinary study of the final episode of the Manda Hararo dyke sequence, Ethiopia, and implications for trends in volcanism during the rifting cycle. *Special Publication*, *420*(1), 149–163. https://doi.org/10.1144/SP420.6

Bialas, R. W., Buck, W. R., & Qin, R. (2010). How much magma is required to rift a continent? *Earth and Planetary Science Letters*, *292*(1–2), 68–78. https://doi.org/10.1016/j.epsl.2010.01.021

Birhanu, Y., Bendick, R., Fisseha, S., Lewi, E., Floyd, M., King, R., & Reilinger, R. (2016). GPS constraints on broad scale extension in the Ethiopian Highlands and Main Ethiopian Rift. *Geophysical Research Letters*, *43*(13), 6844–6851. https://doi.org/10.1002/2016GL069890

Bown, J. W., & White, R. S. (1995). Effect of finite extension rate on melt generation at rifted continental margins. *Journal of Geophysical Research*, *100*(B9), 18011–18029. https://doi.org/10.1029/94JB01478

Brune, S., Williams, S. E., Butterworth, N. P., & Müller, R. D. (2016). Abrupt plate accelerations shape rifted continental margins. *Nature*, *536*(7615), 201–204. https://doi.org/10.1038/nature18319

Calais, E., d'Oreye, N., Albaric, J., Deschamps, A., Delvaux, D., Déverchere, J., et al. (2008). Strain accommodation by slow slip and dyking in a youthful continental rift, East Africa. *Nature*, *456*(7223), 783–787. https://doi.org/10.1038/nature07478

Cervelli, P., Segall, P., Amelung, F., Garbeil, H., Meertens, C., Owen, S., et al. (2002). The 12 September 1999 upper east rift zone dike intrusion at Kilauea volcano, Hawaii. *Journal of Geophysical Research*, *107*(B7), ECV3-1–ECV3-13. https://doi.org/10.1029/2001JB000602

Copernicus Sentinel data. (2024). Copernicus Sentinel data [Dataset]. Retrieved from https://search.asf.alaska.edu/#/

Ebinger, C. J., & Casey, M. (2001). Continental breakup in magmatic provinces: An Ethiopian example. *Geology*, *29*(6), 527–530. https://doi.org/10.1130/0091-7613(2001)029<0527:CBIMPA>2.0.CO;2

Farr, T. G., Rosen, P. A., Caro, E., Crippen, R., Duren, R., Hensley, S., et al. (2007). The shuttle radar topography mission. *Reviews of Geophysics*, *45*(2), RG2004. https://doi.org/10.1029/2005RG000183

Fontijn, K., McNamara, K., Tadesse, A. Z., Pyle, D. M., Dessalegn, F., Hutchison, W., et al. (2018). Contrasting styles of post-caldera volcanism along the Main Ethiopian Rift: Implications for contemporary volcanic hazards. *Journal of Volcanology and Geothermal Research*, *356*, 90–113. https://doi.org/10.1016/j.jvolgeores.2018.02.001

Goldstein, R. M., & Werner, C. L. (1998). Radar interferogram filtering for geophysical applications. *Geophysical Research Letters*, *25*(21), 4035–4038. https://doi.org/10.1029/1998GL900033

Goldstein, R. M., Zebker, H. A., & Werner, C. L. (1988). Satellite radar interferometry: Two-dimensional phase unwrapping. *Radio Science*, *23*(4), 713–720. https://doi.org/10.1029/RS023i004p00713

Grandin, R., Jacques, E., Nercessian, A., Ayele, A., Doubre, C., Socquet, A., et al. (2011). Seismicity during lateral dike propagation: Insights from new data in the recent Manda Hararo–Dabbahu rifting episode (Afar, Ethiopia). *Geochemistry, Geophysics, Geosystems*, *12*(4), Q0AB08. https://doi.org/10.1029/2010GC003434

Hanks, T. C., & Kanamori, H. (1979). A moment magnitude scale. *Journal of Geophysical Research*, *84*(B5), 2348–2350. https://doi.org/10.1029/JB084iB05p02348

Harris, W. C. (1844). *Highlands of Ethiopia*. In J. Winchester, New World Press.

Institut de physique du globe de Paris (IPGP) and Ecole et Observatoire des Sciences de la Terre de Strasbourg (EOST). (1982). GEOSCOPE, French global network of broad band seismic stations [Dataset]. *Institut de physique du globe de Paris (IPGP), Université de Paris*. https://doi.org/10.18715/GEOSCOPE.G

Keir, D., Ebinger, C. J., Stuart, G. W., Daly, E., & Ayele, A. (2006). Strain accommodation by magmatism and faulting as rifting proceeds to breakup: Seismicity of the northern Ethiopian rift. *Journal of Geophysical Research*, *111*(B5), B05314. https://doi.org/10.1029/2005JB003748

Keir, D., Hamling, I. J., Ayele, A., Calais, E., Ebinger, C., Wright, T. J., et al. (2009). Evidence for focused magmatic accretion at segment centers from lateral dike injections captured beneath the Red Sea rift in Afar. *Geology*, *37*(1), 59–62. https://doi.org/10.1130/G25147A.1

La Rosa, A., Pagli, C., & Keir, D. (2024). InSAR csk data of the Fentale dike intrusion of September–October 2024 [Dataset]. *Open Science Framework*. https://doi.org/10.17605/OSF.IO/VDK8Q

La Rosa, A., Raggiunti, M., Pagli, C., Keir, D., Wang, H., & Ayele, A. (2023). Extensional earthquakes in the absence of magma in northern Afar: Insights from InSAR. *Geophysical Research Letters*, *50*(10), e2023GL102826. https://doi.org/10.1029/2023GL102826

Maguire, P. K. H., Keller, G. R., Klemperer, S. L., Mackenzie, G. D., Keranen, K., Harder, S., et al. (2006). Crustal structure of the northern Main Ethiopian Rift from the EAGLE controlled-source survey; a snapshot of incipient lithospheric break-up. *Geological Society, London, Special Publications*, *259*(1), 269–292. https://doi.org/10.1144/GSL.SP.2006.259.01.21

NASA Shuttle Radar Topography Mission (SRTM). (2013). Shuttle radar topography mission (SRTM) global [Dataset]. *Distributed by OpenTopography*. https://doi.org/10.5069/G9445JDF

Okada, Y. (1985). Surface deformation due to shear and tensile faults in a half-space. *Bulletin of the Seismological Society of America*, *75*(4), 1135–1154. https://doi.org/10.1785/BSSA0750041135

Qin, R., & Buck, W. R. (2008). Why meter-wide dikes at oceanic spreading centers? *Earth and Planetary Science Letters*, *265*(3–4), 466–474. https://doi.org/10.1016/j.epsl.2007.10.044

Quinteros, J., Strollo, A., Evans, P. L., Hanka, W., Heinloo, A., Hemmleb, S., et al. (2021). The GEOFON program in 2020 [Dataset]. *Seismological Research Letters*, *92*(3), 1610–1622. https://doi.org/10.1785/0220200415

Raggiunti, M., Keir, D., Pagli, C., & Lavayssière, A. (2023). Evidence of fluid induced earthquake swarms from high resolution earthquake relocation in the Main Ethiopian Rift. *Geochemistry, Geophysics, Geosystems*, *24*(4), e2022GC010765. https://doi.org/10.1029/2022GC010765

Rosen, P. A., Gurrola, E. M., Sacco, G. F., & Zebker, H. (2012). The InSAR scientific computing environment [Software]. In *EUSAR 2012; 9th European conference on synthetic aperture radar* (pp. 730–733). Retrieved from https://github.com/isce-framework/isce2

Siegburg, M., Gernon, T. M., Keir, D., Bull, J. M., Taylor, R. N., Watts, E. J., et al. (2023). Temporal clustering of fissural eruption across multiple segments within the Ethiopian Rift. *Frontiers in Earth Science*, *11*, 1169635. https://doi.org/10.3389/feart.2023.1169635

Sigmundsson, F., Parks, M., Geirsson, H., Hooper, A., Drouin, V., Vogfjörd, K. S., et al. (2024). Fracturing and tectonic stress drive ultrarapid magma flow into dikes. *Science*, *383*(6688), 1228–1235. https://doi.org/10.1126/science.adn283

Temtime, T., Biggs, J., Lewi, E., & Ayele, A. (2020). Evidence for active rhyolitic dike intrusion in the northern Main Ethiopian Rift from the 2015 Fentale seismic swarm. *Geochemistry, Geophysics, Geosystems*, *21*(6), e2019GC008550. https://doi.org/10.1029/2019GC008550

The MathWorks Inc. (2022). MATLAB version: 9.13.0 (R2022b) [Software]. *The MathWorks Inc*. Retrieved from https://www.mathworks.com

United States Geological Survey. (2024). Earthquake lists, maps, and statistics [Dataset]. Retrieved from https://www.usgs.gov/natural-hazards/earthquake-hazards/lists-maps-and-statistics

Wang, H., Wright, T. J., Yu, Y., Lin, H., Jiang, L., Li, C., & Qiu, G. (2012). InSAR reveals coastal subsidence in the Pearl River Delta, China [Software]. *Geophysical Journal International*, *191*(3), 1119–1128. https://doi.org/10.1111/j.1365-246X.2012.05687.x

Weston, J., Ferreira, A. M. G., & Funning, G. J. (2012). Systematic comparisons of earthquake source models determined using InSAR and seismic data. *Tectonophysics*, *532–535*, 61–81. https://doi.org/10.1016/j.tecto.2012.02.001

Wessel, P., Luis, J. F., Uieda, L., Scharroo, R., Wobbe, F., Smith, W. H. F., & Tian, D. (2019). The generic mapping tools version 6 [Software]. *Geochemistry, Geophysics, Geosystems*, *20*(11), 5556–5564. https://doi.org/10.1029/2019GC008515

Williams, F. M., Williams, M. A. J., & Aumento, F. (2004). Tensional fissures and crustal extension rates in the northern part of the Main Ethiopian Rift. *Journal of African Earth Sciences*, *38*(2), 183–197. https://doi.org/10.1016/j.jafrearsci.2003.10.007

Wolfenden, E., Ebinger, C., Yirgu, G., Deino, A., & Ayalew, D. (2004). Evolution of the northern Main Ethiopian rift: Birth of a triple junction. *Earth and Planetary Science Letters*, *224*(1–2), 213–228. https://doi.org/10.1016/j.epsl.2004.04.022

Wright, T. J., Ebinger, C., Biggs, J., Ayele, A., Yirgu, G., Keir, D., & Stork, A. (2006). Magma-maintained rift segmentation at continental rupture in the 2005 Afar dyking episode. *Nature*, *442*(7100), 291–294. https://doi.org/10.1038/nature04978